THE JOURNAL OF PHYSICAL CHEMISTRY Letters

Perspective

pubs.acs.org/JPCL

Developing Plasmonics Under the Infrared Microscope: From Ni Nanoparticle Arrays to Infrared Micromesh

Marvin A. Malone, Antriksh Luthra, David Lioi, and James V. Coe*

Department of Chemistry, The Ohio State University, 100 West 18th Avenue, Columbus, Ohio 43210-1173, United States

ABSTRACT: Microscopes typically collect light over large ranges of angles dispersing plasmonic resonances. While this is an advantage for recording spectra of microscopic particles, it is a disadvantage for sensing by resonance shifts. Adaptations are described herein which enable one to identify, manipulate, and examine narrow plasmonic resonances under a microscope. Noting more general familiarity with metal nanoparticle arrays, a useful perspective is offered by relating the optical transmission of small Ni nanoparticle arrays to that of Ni metal films with microhole arrays, i.e., infrared-active mesh. This perspective also includes the connection to traditional dispersion studies, a new microscope method to measure the propagation length of surface-plasmon-polariton-mediated resonances, and the shifting of resonance positions by latex microspheres in the holes of mesh.

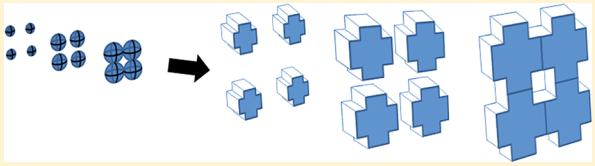

Adaptations are described herein which enable one to identify, manipulate, and examine narrow plasmonic resonances under a microscope.

The large range of angles typically collected by microscopes can be a severe shortcoming when working with plasmonic resonances. The large angle range results in resonance dispersion (spreading out of resonance position) and diminished intensity.In the future, the following line of work may lead to an IR microscope designed for plasmonics. This would be an IR microscope better able to study subwavelength size particles. Simple modifications are described herein that enable one to identify, manipulate, and examine narrow plasmonic resonances under a microscope.

Plasmonics in the infrared (IR) using Ni films with arrays of microholes (mesh) is generally less familiar than the localized surface plasmon resonances of isolated metal nanoparticles, so this Perspective starts by establishing a relationship between the plasmonic transmission of an array of Ni nanoparticles and that of a Ni micromesh. While Ni is not considered a good plasmonic metal in the visible region, the plasmonic nature of the transmission spectrum of a Ni nanoparticle array can be illustrated as the part that changes when the nanoparticle width is increased relative to the lattice parameter - other parts arise simply from the bulk Ni dielectric function. By increasing the nanoparticle width until the nanoparticles touch, the nanoarray becomes a mesh, i.e., a metal film with an array of holes. One might say that the mesh is a highly coupled array of metal particles. This sequence involves the transformation of a capacitive grid of metal particles into an inductive grid (hole array in a metal film). Therefore the process might also be viewed in terms of Babinet's principle,[1−3] i.e., the resulting mesh has a conjugate structure that is an array of metal particles (change holes into metal and metal into space), and one expects a relationship between the reflection and transmission of conjugate pairs. Then, the whole process is moved into the IR region by increasing the lattice parameter and changing the shape of the particle. Cross-like Ni particles grow directly into our IR mesh (a square microlattice with square holes) that has been used in many studies.[4−7] Dispersion measurements and momentum matching equations are presented that characterize the IR plasmonic nature of the Ni microarrays as adapted to measurement with an imaging IR microscope. Finally, examples of resonance characterization and particle sensing are presented using mesh under the IR microscope.

Ni Nanoparticle Arrays. The plasmonics of a single spherical metal nanoparticle is well understood in terms of a localized surface plasmon.[8−11] The extinction resonance is most simply modeled with Mie theory[9,11,12] for spherical particles and arises at the wavelength in which the real part of the metal's dielectric function (ε'_m) equals −2 (when the imaginary component, ε''_m, is negligible). Unlike Au, Ag, and Cu, which are considered good plasmonic materials in the visible, Ni is not considered good[13] because $|\varepsilon'_m| < \varepsilon''_m$ in the visible, as based on smooth metal considerations.[14] An array of very small Ni nanoparticles can be expected to have an extinction spectrum related to the bulk absorption spectrum. Experimental studies by Amekura and co-workers[15,16] observed Ni nanoparticle spectra with absorptions similar to bulk, and they provide an interesting discussion of the plasmonic nature of these transitions. Alternatively, as a nanoparticle is incorporated into an ordered nanoarray, interactions between particles can be observed. Schatz and co-workers have predicted distortions of extinction spectra due to coupling between adjacent metal nanoparticles[17] in two-dimensional ordered arrays. One notable difference of these transitions from bulk concerns a shifting with particle radius.

Received: April 23, 2012
Accepted: June 14, 2012
Published: June 14, 2012

   dx.doi.org/10.1021/jz300499a | *J. Phys. Chem. Lett.* 2012, 3, 1774−1782

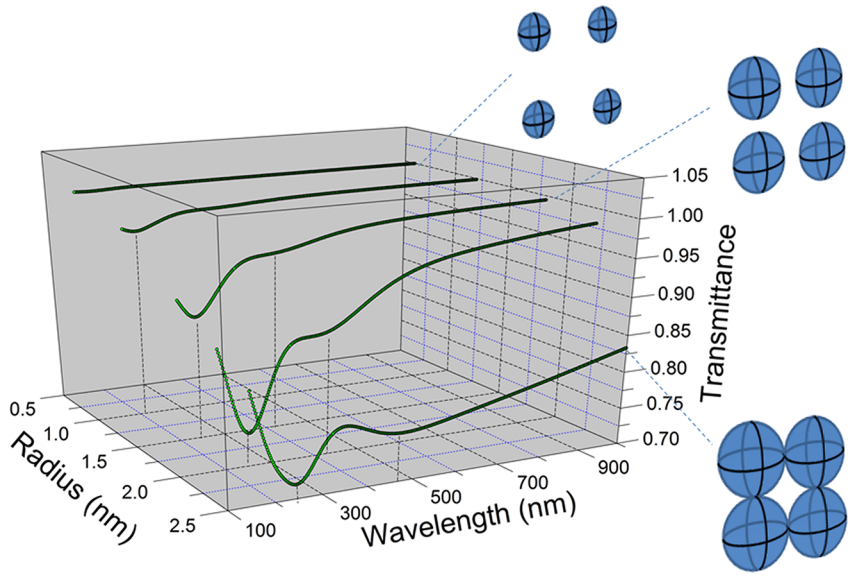

Figure 1. 3D-FDTD calculations of the transmittance of an array of spherical Ni nanoparticles on a 5 nm, square lattice as the radius of the particles increases. The drawings show how the spherical nanoparticles grow until, at a radius of 2.5 nm, they touch making a mesh. The extinction peak in the 400−500 nm range redshifts and broadens with stronger coupling.

The transmission spectra of Ni nanoparticles of various radii on a 5 nm square lattice array have been computed by us with a three-dimensional, finite difference time domain (3D-FDTD) simulation using Lumerical's software (5 nm × 5 nm × 80 nm cell, 0.00038 fs step, nonuniform gridding, Palik's Ni dielectric function, periodic boundary conditions along the mesh, and absorbing PML settings for incident direction, $k = 0$, which is perpendicular incidence).[18] The results are shown in Figure 1, where the particle radius has values of 0.6, 1.2, 1.8, 2.2, and 2.5 nm, the last being the size at which the nanoparticles touch becoming a mesh. Each spectrum shows a downward peak at ∼200 nm (∼6.2 eV) with extinction roughly linear to particle volume, which is like the bulk absorption spectrum. However, as the particles become larger, or the gap between the particles becomes smaller, the plasmonic coupling increases, and there is a second peak that tunes to longer wavelength with stronger coupling. Conversely, since this peak is changing, it cannot be directly or fully due to the bulk absorption. A red shift with stronger coupling is taken as an indication of the plasmonic nature of this extinction resonance as characterized in the work of Schatz and co-workers.[17] This coupling behavior has been observed experimentally by Murray et al,[19] using metal nanoparticle arrays with a lattice parameter in the visible.

A useful perspective is offered by relating the optical transmission of small Ni nanoparticle arrays to that of Ni metal films with microhole arrays, i.e., infrared-active mesh.

Ni Micromesh. The same strategy of particles growing on a fixed lattice is employed to obtain our standard IR mesh with which many experiments[4−7] have been performed. The lattice parameter is increased to 12.7 μm (from 0.005 μm), and the shape of the Ni particles is changed to a cross of two overlapping and identical rectangles, each with a length that is 1.649 times the width (a), and having a constant thickness of 2 μm (see insets in Figure 2). Such a sequence grows into a mesh with 5.0 μm square holes when the gap is zero. The IR transmission spectra were again computed with 3D-FDTD simulations (12.7 μm × 12.7 μm × 100 μm cell, 0.19 fs step, nonuniform gridding, Palik's Ni dielectric function, periodic boundary conditions along the mesh and absorbing PML settings for incident direction, $k = 0$, which is perpendicular incidence)[18] and are presented in Figure 2, where the width (a) of the cross was 1.2, 1.8, 3.0, 4.25, 5.5, 6.7, and 7.7 μm producing a gap of 10.7, 9.7, 7.8, 5.7, 3.6, 1.2, and 0.0 μm, respectively. At the smaller particle or large gap sizes, there is a single, down-going peak at about 12.7 μm which is due to destructive interference (as first noted by Lord Rayleigh on gratings).[20,21] Unlike a metal nanoparticle array, which has an extinction resonance near the wavelength when $\varepsilon'_m = -2$ (allowing for coupling), this extinction of the microarray is governed by the lattice parameter. Notice that at intermediate gap sizes, there are extra, broad peaks at longer wavelengths. These peaks shift with changing gap size and are due to plasmonic coupling − just as seen with the nanoparticle sequence. However, something dramatically different occurs as the gap closes. While all features to this point have been extinctions (losses of transmission), there is the beginning of an up-going feature at the next-to-smallest gap. Finally, when the gap is zero (our standard IR mesh), there is a strong and narrow up-going resonance of 72% transmission at 13.1 μm.

In fact, there are resonances like this for each of the diffraction spots that are transmitted by mesh at shorter wavelengths.[5,22] At increasingly longer wavelengths, these spots are bent to larger angles. When the light (that would produce spots at shorter wavelengths) is bent parallel to the surface, then the light is no longer transmitted normally, and it interacts with the conducting electrons of the metal creating surface plasmon polaritons that mediate and label observed transmission resonances. Further coupling with the modes of the holes produces transmission without scattering from the incident beam, i.e. Ebbesen's extraordinary transmission[23] effect pushed into the IR. In fact, this effect may have first been observed in the far-infrared region

dx.doi.org/10.1021/jz300499a | J. Phys. Chem. Lett. 2012, 3, 1774−1782

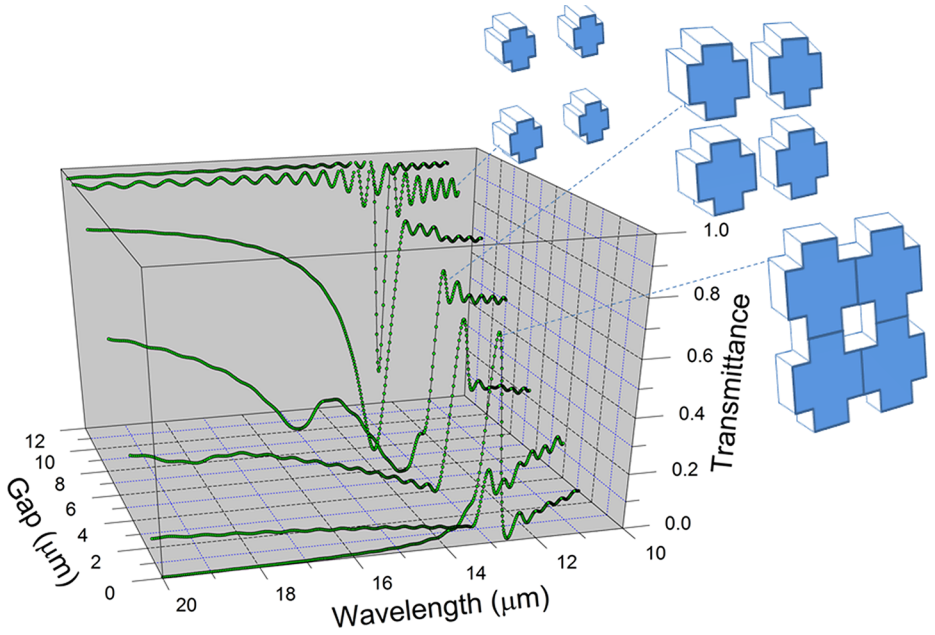

Figure 2. 3D-FDTD calculations of the transmittance of an array of cross-like Ni microparticles on a 12.7 μm square lattice as the particle size increases and the gap decreases. The ratio of the width-to-length of the rectangles comprising the crosses has been set such that our experimental infrared mesh geometry is obtained when the gap is zero. Coupling effects (red-shifted and broadened extinction peaks) get stronger as the crosses get bigger. The end of the sequence (zero gap or mesh) shows a narrow, up-going, transmission resonance in contrast to the down-going extinctions of the microparticle arrays.

by Ulrich.[1] There is a body of work on grids[3,24,25] and work in the IR on mesh is done by an increasing number of groups.[26−34]

Applications in Chemistry. The Coe Group develops applications for plasmonic micromesh in chemistry. Due to the unusual IR transmission, metal mesh can function as a new window substrate[5,6,13] and has been used to study coatings,[35−37] catalytic reactions in thin films,[38] fundamentals of the resonances,[39−42] and mesh doublestacks.[43] Noting that metal micromesh can collect IR light from a larger area, which is then funneled through a subwavelength hole, it becomes possible, using standard IR imaging microscopes, to take spectra of objects in mesh holes that are smaller than the minimally useful window of ordinary operation. Scatter-free IR absorption spectra of single, subwavelength particles including single live yeast cells,[44] latex spheres,[45] and airborne dust particles[46,47] have been reported. Globular particles of ~4 μm width are among the largest that are breathed into people's lungs, so there is much interest in the chemical identity of such particles.

In the future, the following line of work may lead to an IR microscope designed for plasmonics.

Plasmonic Resonances under the Microscope. A microscope investigates a much smaller region of space with a large range of incident angles in comparison to a benchtop spectrometer. These optical features produce mesh resonances that may be dispersed and broadened beyond utility. Furthermore, sensing by resonance position may be distorted or untenable when the propagation distance of surface-plasmon-mediated resonances becomes comparable to the spatial extent of the region investigated under the microscope. So, it was not at all clear that sensing experiments with narrow propagating resonances were possible under a microscope. In this section, it is shown that resonances can be obtained under the microscope that are sufficiently narrow for identification and dispersion studies. Later, the sensing of subwavelength particles is demonstrated.

Our techniques to enable plasmonic sensing studies with an IR microscope[48] start with plasmonic mesh. A typical piece of our IR plasmonic Ni mesh (5 μm wide square holes, 12.7 μm square lattice parameter, 2 μm thick, from Precision Eforming LLC) is shown with a scanning electron microscope image in Figure 3a.

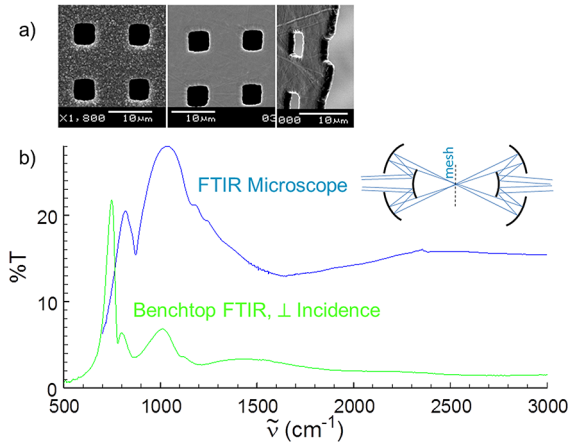

Figure 3. (a) Front, back, and side scanning electron microscope images of a typical Ni mesh. (b) Transmission spectra of the same piece of Ni mesh in a benchtop FTIR at perpendicular incidence and in an FTIR microscope with Cassegrain optics. A schematic of the microscope optics is inset showing the large range of incident angles.

Transmission spectra of such a piece of mesh are shown in Figure 3b using a benchtop FTIR (where the incident light is perpendicular using a small range of angles, green trace) and in an IR imaging microscope (Perkin-Elmer Spotlight 300), where a ring of light in a range from 17° to 37° off of the optical axis

dx.doi.org/10.1021/jz300499a | J. Phys. Chem. Lett. 2012, 3, 1774−1782

is collected due to a system of Cassegrain reflective optics (blue trace, with an inset of the microscope optics). Plasmonic resonances disperse with angle[39,40] which, with the microscope, averages away sharp plasmonic features and produces a better background for spectroscopy. If a 3.2 mm diameter aperture is used 12 mm off-axis and 25 mm below the microscope focal plane[48] (see the right side of Figure 4), then much sharper

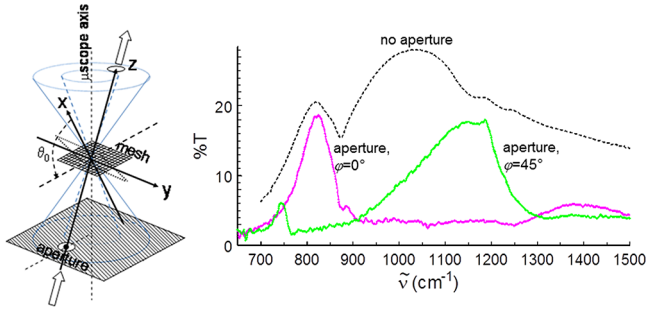

Figure 4. A graphic (left) showing the FTIR microscope-aperture system and definition of a coordinate system at the mesh sample relative to the off-axis aperture. Transmission spectra of Ni mesh are shown (at right) with no aperture (black, dotted trace), with the mesh aligned with the aperture ($\varphi = 0°$, pink solid trace), and rotated by $\varphi = 45°$ about the microscope axis (green solid trace). The resonances are much narrower with the aperture, and the resonances shift significantly with different values of φ, showing that this is a useful coordinate for dispersion studies.

transmission resonances are observed with the microscope (right side of Figure 4) − ones that disperse in predictable ways. Using the coordinate system defined by the aperture on the left side of Figure 4, rotations about the x, y, and z-axes are taken as the angles γ, θ, and φ, respectively. A useful dispersion coordinate for mesh in the focal plane of a microscope is defined by rotation of the mesh in the focal plane about the microscope optical axis (by the angle φ) as γ and θ are held constant at 0° and ∼28°, respectively. Note how significantly the transmission changes as the mesh is rotated by $\varphi = 45°$ in the microscope with an aperture (Figure 4, right). Many transmission spectra were recorded with successive values of φ and detected with two different orientations of a polarizer (0 and 90°), as shown in Figure 5. Note that previous work was unpolarized. The spectra of Figure 5 were smoothed, and peak maxima were extracted to produce the experimental portion (symbols) of the dispersion diagram of Figure 6.

Modeling the Microscope Dispersion Data. The momentum of light in the space of the mesh as an effective medium ($2\pi\tilde{\nu}n_{eff}$) can be equated to the momentum components of light (k_x and k_y) and grating contributions ($2\pi i/L$ and $2\pi j/L$) at the mesh by the following momentum matching relation:

$$(2\pi\tilde{\nu}n_{\text{eff}})^2 = \left(k_x + \frac{2\pi i}{L}\right)^2 + \left(k_y + \frac{2\pi j}{L}\right)^2 \quad (1)$$

where $k_x = 2\pi\tilde{\nu}$ sin θ cos φ and $k_y = 2\pi\tilde{\nu}$ sin θ sin φ are components of light at the mesh surface, i and j are steps along the reciprocal lattice (indices of diffraction spots that have become resonances), L is the lattice parameter, and n_{eff} is the effective index of refraction that varies with wavenumber as $n_{\text{eff}}(\tilde{\nu}) = \alpha_0 + (\alpha_1/\tilde{\nu})$. In the present case of rotation of mesh about the microscope's optical axis (with an off axis aperture),

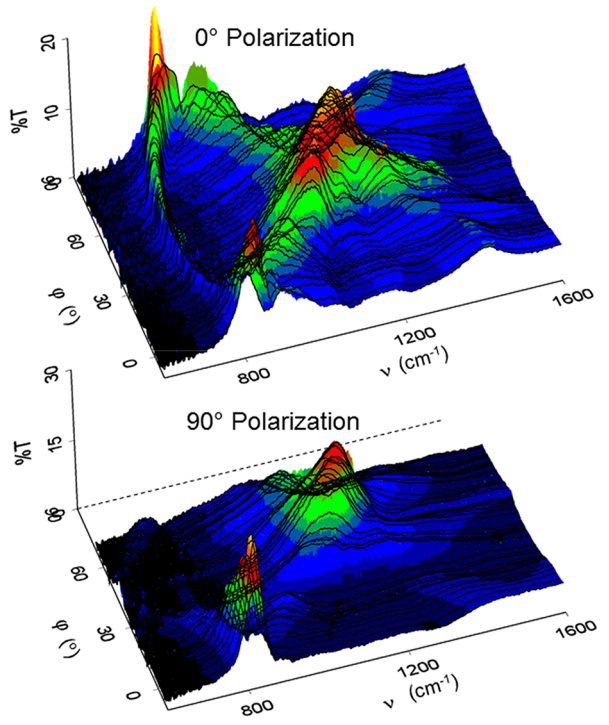

Figure 5. Transmission spectra (top) of mesh with the imaging IR microscope in steps of φ (rotation of the mesh relative to the aperture about the microscope optical axis) from 0° to ∼90° with a polarizer at 0°. Bottom is the same except the polarizer is set at 90°. Many resonance dispersion trends are apparent.

the mesh is at a fixed tilt of $\theta_0 \approx 28°$. Solving the quadratic equation for $\tilde{\nu}$ and allowing n_{eff} to vary with wavenumber gives

$$\tilde{\nu}(i, j, \phi) = \left\{ \frac{2 \sin\theta_0(i \cos\phi + j \sin\phi)}{L} - 2\alpha_0\alpha_1 + \left[\left(2\alpha_0\alpha_1 - \frac{2 \sin\theta_0(i \cos\phi + j \sin\phi)}{L} \right)^2 - 4(\alpha_0^2 - \sin^2\theta_0)\left(\alpha_1^2 - \frac{i^2 + j^2}{L^2}\right) \right]^{1/2} \right\} / [2(\alpha_0^2 - \sin^2\theta_0)] \quad (2)$$

This equation was used to obtain the lines in Figure 6 with simulation parameters of $L = 12.55$ μm, $\theta_0 = 28.5°$, $\alpha_0 = 1.134$, $\alpha_1 = -59.941$, and an offset of +2.0 in φ for the experimental data. One of the most striking features of this dispersion plot is that eight different i,j curves nearly cross at $\varphi = 45°$ and ∼1180 cm^{-1}. While the strongest transmission resonances of a square lattice mesh at perpendicular incidence involve the contributions of only 4 diffraction spots, this geometry (see the left side of Figure 4, i.e., rotated about the y-axis by ∼28° and the optical axis by 45°) amounts to a shift in reciprocal space of half a Brillouin zone in both the x and y directions. This places eight diffraction spots symmetrically about the origin. This prominent feature was called the "monster plasmon" because eight degenerate resonances are likely to give rise to high electromagnetic intensity and strong plasmonic effects, however in practice, the mixture of different states has rendered it less useful than single transitions for sensing applications. Perhaps others will find applications for the monster plasmon.

Polarization effects arise in mesh because it is a bigrating with both horizontal and vertical structure. With smooth metal

dx.doi.org/10.1021/jz300499a | J. Phys. Chem. Lett. 2012, 3, 1774−1782

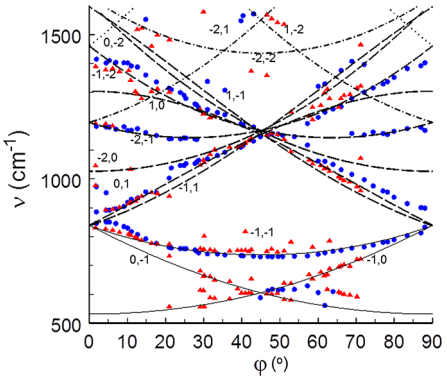

Figure 6. The positions of transmission resonance maxima in Figure 5 are plotted against φ (rotation about the microscope axis relative to the off-axis aperture) producing a φ dispersion plot. The filled circles are 0° polarization and the open circles are 90° polarization. A correction offset of +2.0 in φ was added as determined by folding the data at $\varphi = 45°$. The lines that simulate the data were calculated using the momentum matching relations of eq 2 and the parameters: $L = 12.55$ μm, $\theta_0 = 28.5°$, $\alpha_0 = 1.134$, and $\alpha_1 = -59.941$. The near overlap of eight different pairs of lines at $\varphi = 45°$ and $\tilde{\nu} = 1180$ cm^{-1} produces a resonance that we call the "monster plasmon". The positions of these resonances are well-predicted by momentum matching.

surfaces, propagation directions of surface plasmon polaritons will follow the incident polarization, but mesh holes can point surface plasmon polaritons in various directions. The most marked differences due to polarization were evident in the lowest energy resonances at $\varphi = 45°$, as shown in Figure 7. These effects went unobserved in our earlier, unpolarized work.[48] Unpolarized work shows two low energy resonances (610 and 735 cm^{-1} at $\varphi = 45°$); however, a polarizer can select one or the other resonance as shown in Figure 7a. The peak heights of these two transmission resonances were measured as a function of polarization as shown in Figure 7b. These two resonances are 90° out of phase with each other. Each disappears while the other is maximized. Nonlinear least-squares fits with sin^2 and cos^2 functions are given in Figure 7b as traces.

It is often useful to display dispersion measurements as a function of momentum in k-space, i.e., a formal connection with other dispersion work is provided. Our microscope-with-aperture geometry involves varying both k_x and k_y; however, their sum is constrained by φ, rotation about the microscope axis, as

$$k_x + k_y = 2\pi\tilde{\nu} \sin\theta_0(\cos\phi + \sin\phi) \quad (3)$$

where θ_0 is the fixed tilt about the y-axis. The same data that are presented in Figure 6 are presented in k-space in Figure 8 with filled symbols. The solid green lines represent mesh rotation at $\varphi = 0°$ and $\varphi = 45°$. The data recorded between $\varphi = 45°$ and 90°, fold back into the space between the green lines with $\varphi = 90°$ being the same as $\varphi = 0°$. The open symbols are the experimental data projected to the $\varphi = 90$–$180°$ region. The solid black curves are the same momentum matching curves as shown in Figure 6. The dashed lines represent the light line folded into this wave vector space. Note the crossing of four sets of lines near $\varphi = 0°$ and 850 cm^{-1}, and the crossing of eight sets of lines near $\varphi = 45°$ and 1180 cm^{-1}. The experimental data, which involve light interacting with the metal surface, exhibit avoided crossings and significant shifts from the light line in contrast to light, by itself. When light interacts with the conducting electrons of the metal, the resulting mixed state (or polariton) takes on some fermionic character, and the resonances interact to some extent like molecules, rather than light.[49]

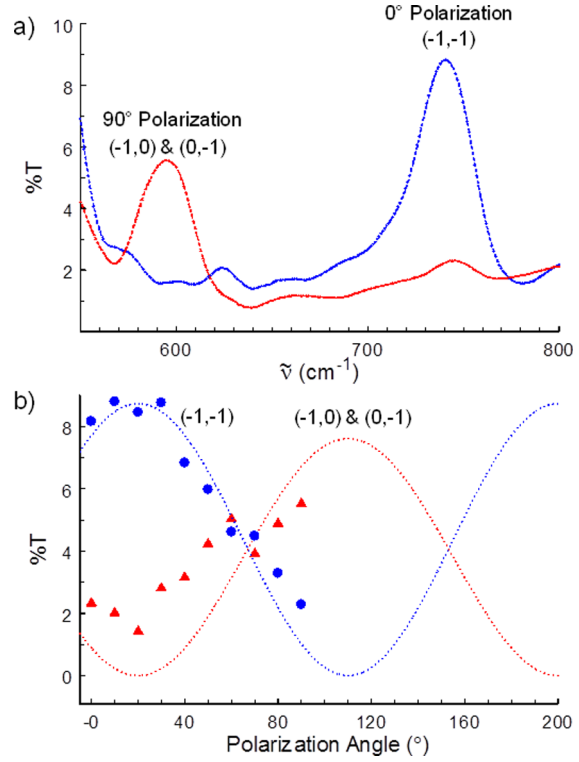

Figure 7. (a) IR microscope transmission spectra of mesh rotated by $\varphi = 45°$ in the low energy region comparing polarization at 0° and 90°. These resonances are very responsive to polarization. (b) Plot (symbols) and fit (solid traces) of the transmission peak maximum ($\%T$) as a function of polarization angle for the same low energy resonances seen above in part (a). The two peaks are 90° out of phase and follow simple trigometric cos^2 or sin^2 functions.

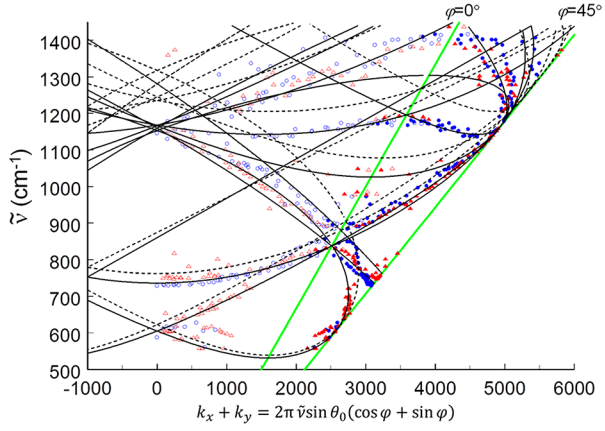

Figure 8. Resonance peak position is plotted versus the sum of the k_x and k_y wavevectors, which can be given in terms of the single variable φ. This produces a momentum dispersion plot in k-space. The space between the solid green lines corresponds to data collected from $\varphi = 0°$ to 90°, but the data from 45–90° folds back into the 0–45° region. All experimental data has an offset of +2.0 in φ as determined by folding the data. The filled blue circles are 0° polarization and the filled red triangles are 90° polarization. The open symbols are a projection of the experimental data into the region of $\varphi = 90$–$180°$. The solid lines are momentum matching curves calculated using eq 2 and $L = 12.55$ μm, $\theta_0 = 28.5°$, $\alpha_0 = 1.134$, and $\alpha_1 = -59.941$. The dashed lines are the light line ($n_{\text{eff}} = 1.000$) folded into momentum space.

Resonance Propagation Lengths by Microscope Window. The infrared microscope's variable aperture, which selects the

dx.doi.org/10.1021/jz300499a | J. Phys. Chem. Lett. 2012, 3, 1774–1782

sampled area or window, can be made comparable in size to the propagation distance of some plasmonic transmission resonances. Since this affects the resonance transmission intensity, a study of resonance transmission versus window size can be used to characterize the resonance propagation distance along the mesh. However, the variable aperture works against an effective fixed aperture of 100 × 100 μm^2 in our instrument, so there is a practical upper constraint of ~100 μm in this method.

The main resonance at $\varphi = 0°$ and 830 cm^{-1}, was investigated using a wire grid polarizer at 90° and variable windows. One dimension of the window was set at 100 μm, while the other was varied as shown in the Figure 9 insets. The resonance transmission

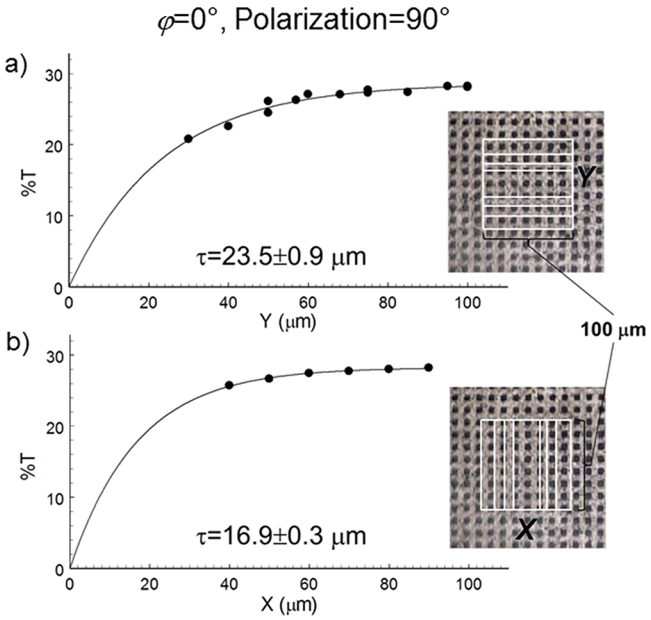

Figure 9. Peak maximum transmission for a resonance (830 cm^{-1}, $\varphi = 0°$, polarizer at 90°) with empty mesh under the IR microscope versus variable microscope window size (X or Y). (a) Plot of resonance maximum transmission versus the vertical dimension of the microscope window (Y). (b) Plot of resonance maximum transmission for a variable change in the horizontal dimension of the microscope window (Y) with the same polarization as in panel a.

(I, in units of % transmission) is plotted in Figure 9 as a function of the variable window width or length. The data was fit with a nonlinear least-squares routine to the following form:

$$I = \beta_0(1 - e^{-W/\beta_1}) \quad (4)$$

where W is the variable length of the window (either X or Y, for horizontal or vertical variations, respectively), β_0 is the large window intensity, and β_1 is the $1/e$ propagation distance. The propagation length is 23.5 ± 0.9 μm for the vertical, Y, direction and 16.9 ± 0.3 μm for the horizontal, X, direction with the polarizer commonly fixed. These distances are a factor of 1.85 and 1.33 of the lattice parameter (12.7 μm), respectively. These results are in rough agreement with our previous results[41] yielding a $1/e$ propagation length (by absorption from a ring of latex spheres) of 17.8 ± 2.9 μm. While surface plasmon polaritons may run much larger distances on smooth metal surfaces,[14] damping at the next hole is a defining mechanism of the plasmonic resonances on infrared-active mesh. This type of damping is not a loss; rather the light largely rejoins the incident beam and is useful in transmission studies.

Particle Sensing. The transmission resonance can be sensitive to the surrounding environment. In the simplest case, a change in the effective refractive index should result in red-shifted resonances. A complete submersion of the mesh in a dielectric material maximally shifts the resonance by a factor of $1/n_{eff}$. However, particles will cause shifts dependent on the amount and position of the material, as can be observed under the IR microscope. The (−1,−1) resonance was chosen to sense the presence of polystyrene microspheres in the holes of mesh because this resonance is narrow (inherently <25 cm^{-1}) and appears in some parts of momentum space as a single resonance (near $\varphi = 45°$). The polystyrene microspheres, obtained from SPI Supplies, are 5.0 ± 0.4 μm in diameter with a 1.58 refractive index (at 540 nm). The (−1,−1) resonance in air is peaked at 735 cm^{-1} and theoretically should shift to 465 cm^{-1} if fully submersed in polystyrene. A 3D-FDTD calculation[18] at perpendicular incidence with all holes filled with microspheres showed that the main resonance shifts ~100 cm^{-1}, so shifts were measured in the IR microscope with variable fractions of holes filled with latex microspheres as shown in Figure 10. The effective fixed aperture

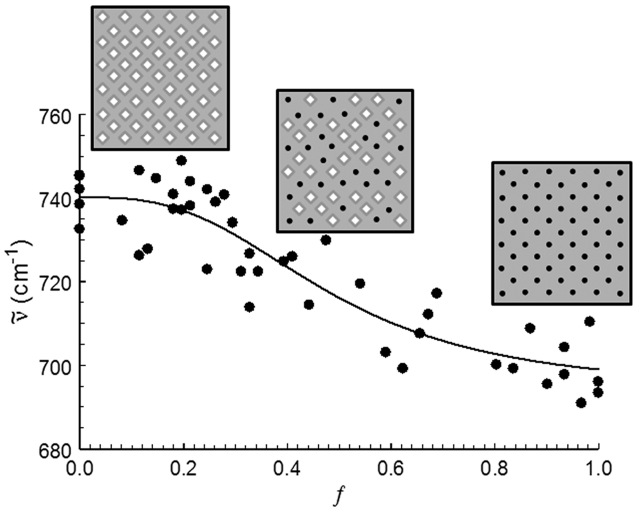

Figure 10. Position (filled symbols) of the (−1,−1) resonance at $\varphi = 45°$ with a polarizer at 15° as a function of the fraction of mesh holes filled by 5 μm diameter latex microspheres within a 100 μm × 100 μm window. There are 61 holes to be filled in this window. The inset drawings show all empty holes, 15 holes filled, and all holes filled. Although the holes have been filled randomly for this experiment, clearly the resonance shifts to lower wavenumber as holes are filled. The solid trace is fit to a logistic sigmoid functional form, ignoring the large scatter due to coupling between spheres in adjacent holes.

of 100 × 100 μm^2 sampled 61 mesh holes, so the fractions are out of 61. To reduce the interaction with the resonance at 610 cm^{-1}, the mesh was rotated to $\varphi = 45°$, and a polarizer was used to obtain the largest intensity (15°). A maximum shift of about 50 cm^{-1} was observed when all 61 holes are filled with polystyrene microspheres. This is only half of the shift expected at perpendicular incidence. Perhaps the difference is due to the sampling angle of the aperture/microscope system. A nonlinear least-squares routine was used to fit the data to a logistic sigmoid function of the form

$$\tilde{\nu}_p(f) = \frac{\tilde{\nu}_{empty} - \tilde{\nu}_{filled}}{1 + \left(\frac{f}{b}\right)^P} + \tilde{\nu}_{filled} \quad (5)$$

dx.doi.org/10.1021/jz300499a | J. Phys. Chem. Lett. 2012, 3, 1774−1782

where $\tilde{\nu}_{empty}$ =740.2 ± 2.3 μm and $\tilde{\nu}_{filled}$ = 694.0 μm (fixed) are the wavenumbers for the empty and filled mesh conditions, f is the fraction of the 61 holes filled, b = 0.49 ± 0.04 is the point of inflection, and P = 2.9 ± 0.5 determines the sharpness of the transition. There is a large scatter in this result because the fractions investigated were randomly arranged, which does not control for coupling between nearby particles. The result shows that shifts are observable, and it will be worthwhile to pursue more controlled arrangements in the future.

Conclusions and Future Work. It is our hope that this work may lead to an IR microscope designed for plasmonic studies and plasmonic imaging, i.e., imaging based on the magnitude of the shift of plasmonic resonances. With the present system, observation of plasmonic resonances involves eliminating a large fraction (~90%) of a normal microscope's incident light by means of an aperture. It would seem possible to design an optical system in which a comparable intensity is confined to a small range of k-values about a single, nonzero value of k. This would be an IR microscope better able to study subwavelength size particles. Ultimately with imaging IR microscopes, it might be possible to develop IR analogues to optical surface plasmon resonance (SPR) sensor arrays.

In conclusion, infrared-active micromesh behaves in several ways like a highly coupled array of metal particles, namely, it shows characteristic shifting of resonances as a function of coupling between adjacent holes or particles. Such coupling amounts to propagation of light along the surface of the mesh; however, the propagation is strongly damped by the presences of holes (the propagation distance is between one and two holes). However, the important aspect is that the damped radiation is not lost. Rather, it emerges from the mesh with little scattering, differing little from the incident beam − at least for the purposes of Fourier transform infrared spectroscopy.A piece of metal micromesh in an IR imaging microscope can be used to record the scatter-free spectrum of a single isolated, subwavelength particle or to sense such particles by the shift of plasmonic resonances. The new microscopic capabilities for plasmonics in the infrared invite comparison to our macroscopic understanding of such phenomena.

A piece of metal micromesh in an IR imaging microscope can be used to record the scatter-free spectrum of a single isolated, subwavelength particle or to sense such particles by the shift of plasmonic resonances.

AUTHOR INFORMATION

Corresponding Author

*E-mail: coe.1@osu.edu.

Notes

The authors declare no competing financial interest.

Biographies

James Coe received his B.A. with Honors in 1980 from Swarthmore College and his Ph.D. in 1986 from The Johns Hopkins University (advisor Kit H. Bowen). Postdoctoral work was done at the University of California, Berkeley (advisor Richard J. Saykally). He is a Professor of Chemistry at The Ohio State University and has been there since 1989. Interests include the optical physics and applications of subwavelength hole arrays in chemistry and spectroscopy, the connection of the properties of finite size materials, such as clusters, to bulk, and detecting cancer with imaging infrared spectra of tissue samples. http://chemistry.osu.edu/faculty/coe

Marvin Malone received his B.S. in Chemistry in 2007 from California State University Dominguez Hills and his M.S. in Chemistry in 2010 from The Ohio State University. He is a fifth-year Ph.D. candidate in chemistry working with Dr. James Coe. His current projects include characterizing plasmonic mesh under an FTIR microscope and using infrared spectroscopy to study particulate matter.

Antriksh Luthra is currently a Ph.D. student in Mechanical Engineering studying under Dr. James V. Coe and Dr. Vish Subramaniam at the Ohio State University, Columbus. He received his M.S. (2010) in Aerospace Engineering from the University of Texas at Arlington and B.E. (2007) in Mechanical Engineering from Visvesvaraya Technological University, India. His current research focuses on infrared spectroscopy of trapped airborne dust particles, plasmonic spectra of inkjet spots, and fabrication of plasmonic metal bigratings.

David Lioi is an undergraduate student studying under James V. Coe at The Ohio State University, working toward a B.S. degree in Chemistry and Physics. His current research focuses primarily on modeling the mid-IR spectra of micrometer size particulate matter. He has worked on 3D-FDTD simulations of micro and nano systems, infrared plasmonic dispersion on nickel metal mesh, and calibrating the group's past work on the "Library of 63 Dust Particles".

ACKNOWLEDGMENTS

We thank the National Science Foundation for support of this work under Grant Numbers CHE 0848486 and CHE 0639163.

REFERENCES

(1) Ulrich, R. Far-Infrared Properties of Metallic Mesh and Its Complementary Structure. *Infrared Phys.* **1967**, *7*, 37−55.
(2) De Abajo, F. J. G. Colloquium: Light Scattering by Particle and Hole Arrays. *Rev. Mod. Phys.* **2007**, *79*, 1267.
(3) Minhas, B. K.; Fan, W.; Agi, K.; Brueck, S. R. J.; Malloy, K. J. Metallic Inductive and Capacitive Grids: Theory and Experiment. *J. Opt. Soc. Am. A* **2002**, *19*, 1352−1359.
(4) Coe James, V.; Williams Shaun, M.; Rodriguez Kenneth, R.; Teeters-Kennedy, S.; Sudnitsyn, A.; Hrovat, F. Extraordinary IR Transmission with Metallic Arrays of Subwavelength Holes. *Anal. Chem.* **2006**, *78*, 1384−1390.
(5) Coe, J. V.; Heer, J. M.; Teeters-Kennedy, S.; Tian, H.; Rodriguez, K. R. Extraordinary Transmission of Metal Films with Arrays of Subwavelength Holes. *Annu. Rev. Phys. Chem.* **2008**, *59*, 179−202.
(6) Coe, J. V.; Rodriguez, K. R.; Teeters-Kennedy, S.; Cilwa, K.; Heer, J.; Tian, H.; Williams, S. M. Metal Films with Arrays of Tiny Holes: Spectroscopy with Infrared Plasmonic Scaffolding. *J. Phys. Chem. C* **2007**, *111*, 17459−17472.
(7) Williams, S. M.; Rodriguez, K. R.; Teeters-Kennedy, S.; Shah, S.; Rogers, T. M.; Stafford, A. D.; Coe, J. V. Scaffolding for Nanotechnology: Extraordinary Infrared Transmission of Metal Microarrays for Stacked Sensors and Surface Spectroscopy. *Nanotechnology* **2004**, *15*, S495−S503.
(8) Malinsky, M. D.; Kelly, K. L.; Schatz, G. C.; Van Duyne, R. P. Nanosphere Lithography: Effect of Substrate on the Localized Surface Plasmon Resonance Spectrum of Silver Nanoparticles. *J. Phys. Chem. B* **2001**, *105*, 2343−2350.

(9) Haes, A. J.; Van Duyne, R. P. A Unified View of Propagating and Localized Surface Plasmon Resonance Biosensors. *Anal. Bioanal. Chem.* **2004**, *379*, 920−930.
(10) Brockman, J. M.; Nelson, B. P.; Corn, R. M. Surface Plasmon Resonance Imaging Measurements of Ultrathin Organic Films. *Annu. Rev. Phys. Chem.* **2000**, *51*, 41−63.
(11) Willets, K. A.; Duyne, R. P. V. Localized Surface Plasmon Resonance Spectroscopy and Sensing. *Annu. Rev. Phys. Chem.* **2007**, *58*, 267−297.
(12) Van Duyne, R. P. Physics: Molecular Plasmonics. *Science (Washington, DC, U. S.)* **2004**, *306*, 985−986.
(13) Williams, S. M.; Stafford, A. D.; Rodriguez, K. R.; Rogers, T. M.; Coe, J. V. Accessing Surface Plasmons with Ni Microarrays for Enhanced IR Absorption by Monolayers. *J. Phys. Chem. B* **2003**, *107*, 11871−11879.
(14) Raether, H. *Surface Plasmons on Smooth and Rough Surfaces and on Gratings*; Springer-Verlag: Berlin, 1988.
(15) Amekura, H.; Kitazawa, H.; Umeda, N.; Takeda, Y.; Kishimoto, N. Nickel Nanoparticles in Silica Glass Fabricated by 60 keV Negative-Ion Implantation. *Nucl. Instrum. Methods Phys. Res., Sect. B* **2004**, *222*, 114−122.
(16) Amekura, H.; Takeda, Y.; Kishimoto, N. Criteria for Surface Plasmon Resonance Energy of Metal Nanoparticles in Silica Glass. *Nucl. Instrum. Methods Phys. Res., Sect. B* **2004**, *222*, 96−104.
(17) Zhao, L.; Kelly, K. L.; Schatz, G. C. The Extinction Spectra of Silver Nanoparticle Arrays: Influence of Array Structure on Plasmon Resonance Wavelength and Width. *J. Phys. Chem. B* **2003**, *107*, 7343−7350.
(18) Heer, J. M. FDTD Modeling of the Spectroscopy and Resonances of Thin Films and Particles on Plasmonic Nickel Mesh. Ph.D. Thesis, The Ohio State University, Columbus, OH, 2010.
(19) Murray, W. A.; Astilean, S.; Barnes, W. L. Transition from Localized Surface Plasmon Resonance to Extended Surface Plasmon-Polariton as Metallic Nanoparticles Merge to Form a Periodic Hole Array. *Phys. Rev. B: Condens. Matter* **2004**, *69*, 165407/165401−165407/165407.
(20) Rayleigh, L. Note on the Remarkable Case of Diffraction Spectra Described by Prof. Wood. *Philos. Mag., Series 6* **1907**, *14*, 60−65.
(21) Sarrazin, M.; Vigneron, J.-P.; Vigoureux, J.-M. Role of Wood Anomalies in Optical Properties of Thin Metallic Films with a Bidimensional Array of Subwavelength Holes. *Phys. Rev. B: Condens. Matter Mater. Phys.* **2003**, *67*, 085415/085411−085415/085418.
(22) Vigoureux, J. M. Analysis of the Ebbesen Experiment in the Light of Evanescent Short Range Diffraction. *Opt. Commun.* **2001**, *198*, 257−263.
(23) Ebbesen, T. W.; Lezec, H. J.; Ghaemi, H. F.; Thio, T.; Wolff, P. A. Extraordinary Optical Transmission through Sub-wavelength Hole Arrays. *Nature (London)* **1998**, *391*, 667−669.
(24) McPhedran, R. C.; Maystre, D. On the Theory and Solar Application of Inductive Grids. *Appl. Phys* **1977**, *14*, 1−20.
(25) Derrick, G. H.; McPhedran, R. C.; Maystre, D.; Neviere, M. Crossed Gratings: A Theory and Its Applications. *Appl. Phys.* **1979**, *18*, 39−52.
(26) Moller, K. D.; Sternberg, O.; Grebel, H.; Lalanne, P. Thick Inductive Cross Shaped Metal Meshes. *J. Appl. Phys.* **2002**, *91*, 9461−9465.
(27) Moller, K. D.; Farmer, K. R.; Ivanov, D. V. P.; Sternberg, O.; Stewart, K. P.; Lalanne, P. Thin and Thick Cross Shaped Metal Grids. *Infrared Phys. Technol.* **1999**, *40*, 475−485.
(28) Ming-Wei, T.; Tzu-Hung, C.; Hsu-Yu, C.; Si-Chen, L. Dispersion of Surface Plasmon Polaritons on Silver Film with Rectangular Hole Arrays in a Square Lattice. *Appl. Phys. Lett.* **2006**, *89*, 093102/1−093102/3.
(29) Tsai, M.-W.; Chuang, T.-H.; Meng, C.-Y.; Chang, Y.-T.; Lee, S.-C. High Performance Midinfrared Narrow-Band Plasmonic Thermal Emitter. *Appl. Phys. Lett.* **2006**, *89*, 173116/173111−173116/173113.
(30) Etou, J.; Ino, D.; Furukawa, D.; Watanabe, K.; Nakai, I. F.; Matsumoto, Y. Mechanism of Enhancement in Absorbance of Vibrational Bands of Adsorbates at a Metal Mesh with Subwavelength Hole Arrays. *Phys. Chem. Chem. Phys.* **2011**, *13*, 5817−5823.
(31) Limaj, O.; Lupi, S.; Mattioli, F.; Leoni, R.; Ortolani, M. Midinfrared Surface Plasmon Sensor based on a Substrateless Metal Mesh. *Appl. Phys. Lett.* **2011**, *98*, 091902/1−091902/3.
(32) Mattioli, F.; Ortolani, M.; Lupi, S.; Limaj, O.; Leoni, R. Substrateless Micrometric Metal Mesh for Mid-infrared Plasmonic Sensors. *Appl. Phys. A: Mater. Sci. Process.* **2011**, *103*, 627−630.
(33) Yong-Hong, Y.; Zhi-Bing, W.; Yurong, C.; Desheng, Y.; Jia-Yu, Z.; Xian, Qi, L.; Tie Jun, C. Enhanced Transmission through Metal Films Perforated with Circular and Cross-Dipole Apertures. *Appl. Phys. Lett.* **2007**, *91*, 251105/1−251105/3.
(34) Yong-Hong, Y.; Yurong, C.; Zhi-Bing, W.; Desheng, Y.; Jia-Yu, Z. Optical Transmission Properties of Perforated Metal Films in the Middle-Infrared Range. *Appl. Phys. Lett.* **2009**, *94*, 081118/1−081118/3.
(35) Rodriguez, K. R.; Tian, H.; Heer, J. M.; Coe, J. V. Extraordinary Infrared Transmission Resonances of Metal Microarrays for Sensing Nanocoating Thickness. *J. Phys. Chem. C* **2007**, *111*, 12106−12111.
(36) Rodriguez, K. R.; Tian, H.; Heer, J. M.; Teeters-Kennedy, S. M.; Cilwa, K.; Coe, J. V. Interaction of an Infrared Surface Plasmon with a Molecular Vibration. *J. Chem. Phys.* **2007**, *126*, 151101−151105.
(37) Teeters-Kennedy, S. M.; Rodriguez, K. R.; Rogers, T. M.; Zomchek, K. A.; Williams, S. M.; Sudnitsyn, A.; Carter, L.; Cherezov, V.; Caffrey, M.; Coe, J. V. Controlling the Passage of Light through Metal Microchannels by Nanocoatings of Phospholipids. *J. Phys. Chem. B* **2006**, *110*, 21719−21727.
(38) Williams, S. M.; Rodriguez, K. R.; Teeters-Kennedy, S.; Stafford, A. D.; Bishop, S. R.; Lincoln, U. K.; Coe, J. V. Use of the Extraordinary Infrared Transmission of Metallic Subwavelength Arrays to Study the Catalyzed Reaction of Methanol to Formaldehyde on Copper Oxide. *J. Phys. Chem. B* **2004**, *108*, 11833−11837.
(39) Williams, S. M.; Coe, J. V. Dispersion Study of the Infrared Transmission Resonances of Freestanding Ni Microarrays. *Plasmonics* **2006**, *1*, 87−93.
(40) Williams, S. M.; Stafford, A. D.; Rogers, T. M.; Bishop, S. R.; Coe, J. V. Extraordinary Infrared Transmission of Cu-coated Arrays with Subwavelength Apertures: Hole Size and the Transition from Surface Plasmon to Waveguide Transmission. *Appl. Phys. Lett.* **2004**, *85*, 1472−1474.
(41) Cilwa, K. E.; Rodriguez, K. R.; Heer, J. M.; Malone, M. A.; Corwin, L. D.; Coe, J. V. Propagation Lengths of Surface Plasmon Polaritons on Metal Films with Arrays of Subwavelength Holes by Infrared Imaging Spectroscopy. *J. Chem. Phys.* **2009**, *131*, 061101−061105.
(42) Heer, J. M.; Coe, J. V. 3D-FDTD Modeling of Angular Spread for the Extraordinary Transmission Spectra of Metal Films with Arrays of Subwavelength Holes. *Plasmonics* **2012**, *7*, 71−75.
(43) Teeters-Kennedy, S. M.; Williams, S. M.; Rodriguez, K. R.; Cilwa, K.; Meleason, D.; Sudnitsyn, A.; Hrovat, F.; Coe, J. V. Extraordinary Infrared Transmission of a Stack of Two Metal Micromeshes. *J. Phys. Chem. C* **2007**, *111*, 124−130.
(44) Malone, M. A.; Prakash, S.; Heer, J. M.; Corwin, L. D.; Cilwa, K. E.; Coe, J. V. Modifying Infrared Scattering Effects of Single Yeast Cells with Plasmonic Metal Mesh. *J. Chem. Phys.* **2010**, *133*, 185101−185107.
(45) Heer, J.; Corwin, L.; Cilwa, K.; Malone, M. A.; Coe, J. V. Infrared Sensitivity of Plasmonic Metal Films with Hole Arrays to Microspheres In and Out of the Holes. *J. Phys. Chem. C* **2010**, *114*, 520−525.
(46) Cilwa, K. E.; McCormack, M.; Lew, M.; Robitaille, C.; Corwin, L.; Malone, M. A.; Coe, J. V. Scatter-Free IR Absorption Spectra of Individual, 3−5 Micron, Airborne Dust Particles Using Plasmonic Metal Microarrays: A Library of 63 Spectra. *J. Phys. Chem. C* **2011**, *115*, 16910−16919.
(47) Malone, M. A.; McCormack, M.; Coe, J. V. Single Airborne Dust Particles using Plasmonic Metal Films with Hole Arrays. *J. Phys. Chem. Lett.* **2012**, *20123*, 720−724.

(48) Malone, M. A.; Cilwa, K. E.; McCormack, M.; Coe, J. V. Modifying an Infrared Microscope to Characterize Propagating Surface Plasmon Polariton-Mediated Resonances. *J. Phys. Chem. C* **2011**, *115*, 12250.
(49) Cilwa, K. E. Surface Plasmon Polaritons and Single Dust Particles. Ph.D. Thesis, The Ohio State University, Columbus, OH, 2011.